16th World Conference on Earthquake, 16WCEE 2017
Santiago Chile, January 9th to 13th 2017
Paper N° 944 (Abstract ID)
Registration Code: S-G1463253119

Full-Scale Cyclic Testing of Deep Slender Wide-Flange Steel Beam-Columns under Unidirectional and Bidirectional Lateral Drift Demands

A. Elkady[1], D. G. Lignos[2]

[1] Post-Doctoral Researcher, Swiss Federal Institute of Technology, Lausanne (EPFL), Switzerland, ahmed.elkady@epfl.ch
[2] Associate Professor, Swiss Federal Institute of Technology, Lausanne (EPFL), Switzerland, dimitrios.lignos@epfl.ch

Abstract

Deep and slender wide-flange steel beam-columns are commonly used in steel special moment frames (SMFs) in North America. These sections provide large moment-of-inertia required to satisfy the design code's drift limits while keeping the column steel weight at minimum. Due to their low out-of-plane moment-of-inertia and high web and flange slenderness ratios, such sections are vulnerable to local and global geometric instabilities when subjected to lateral drift demands coupled with compressive axial load. Past experimental research on steel beam-columns has mainly focused on small and stocky wide-flange sections. To this end, an extensive testing program was conducted at École Polytechnique de Montreal that investigated the cyclic behavior of 10 full-scale deep beam-columns. The column specimens were 600mm deep (i.e., W610 sections). The beam-columns were tested under unidirectional and bidirectional lateral loading protocols coupled with different levels of constant compressive axial load. The test setup involved a 6 degrees-of-freedom control system that was capable of realistically simulating the flexibility of the beam-to-column connection at the top of a first-story beam-column; hence the tests utilized a movable point of inflection during lateral loading as would occur in reality.

This paper discusses the main findings from the experimental program and a corroborating finite element analytical study that investigated the hysteretic behavior of 40 different deep wide-flange beam-columns. In particular, the effects of the local and global slenderness ratio, lateral loading protocol, applied axial load ratios, and boundary conditions on the column's hysteretic behavior were quantified. Furthermore, the effect of bidirectional lateral deformations coupled with compressive axial load on the overall dynamic stability of steel beam-columns is discussed. Finally, out-of-plane forces exerted at the top of the column due to twisting and global buckling about the column's weak-axis are quantified. The quantification of out-of-plane forces is essential to properly design the lateral bracing of steel beam-columns.

Keywords: Deep steel beam-columns, steel moment-resisting frames, full-scale column testing, column axial shortening

1. Introduction

Columns in steel moment-resisting frames (MRF) in North America typically utilize "deep" wide-flange cross-sections, with depth larger than 400 mm (16 in). These members provide a large moment-of-inertia to satisfy various drift requirements for seismic applications [1, 2]. In an effort to reduce the column's weight, designers tend to select "slender" cross-sections, whose local slenderness ratios are close to the limits for highly ductile members [1]. However, deep and slender steel columns are susceptible to local and global instabilities such as local and lateral torsional buckling, respectively.

Uang et al. [3] investigated the cyclic behavior of full-scale W610 (W24) beam-columns. These beam-columns had fixed boundary conditions at both ends (i.e., fixed-fixed) and were mainly tested under unidirectional symmetric lateral loading protocols coupled with a constant compressive axial load. These tests showed that instabilities associated with local and lateral torsional buckling dominated the column response. The tests also showed that seismically compact cross-sections as per [1] with high local slenderness ratios can lose 20% of their maximum flexural capacity at drift ratios less than 3% radians. Similar observations were reported in recent analytical studies [4-6]. Issues associated with bidirectional lateral loading, the employed boundary conditions of the column and the lateral loading protocol have not been addressed but strongly influence the steel column stability under cyclic loading.

To this end, an experimental program was conducted to characterize the cyclic behavior of deep slender beam-columns. The testing program incorporated full-scale W610 (W24) beam-columns with a fixed base and a flexible top. These boundary conditions are representative of first-story steel columns in steel MRFs because the inflection point within the column is not fixed and the flexural, torsional, and warping restraints of the column are not lost simultaneously at both column ends due to capacity design principles (i.e., weak-beam/strong-column ratio). Different types of unidirectional and bidirectional lateral loading protocols, representative of design-basis and collapse-consistent seismic events, were also incorporated as part of the testing program. In order to generalize the findings from the testing program a corroborating analytical study was conducted. This paper discusses some of the main findings of the coordinated experimental and analytical program discussed above. Emphasis is placed on the effects of bidirectional loading, lateral loading type, and local and global slenderness ratios on the cyclic behavior of beam-columns. The out-of-plane forces exerted at the lateral brace of a column at the floor level are also evaluated and compared to the brace design forces as per current design provisions in North America [2, 7].

2. Brief Description of the Testing Program

The testing program was conducted at the structures laboratory of École Polytechnique de Montreal (EPM) using a 6 degrees-of-freedom (DOF) control system. This system is shown in Fig.1. It comprises of 8 actuators connected to a top platen. The 8 actuators can fully-control the 6-DOF (δ_X, δ_Y, δ_Z, θ_X, θ_Y, θ_Z) at the top platen about any control point in space. The control point in this testing program was located at the center of the beam-column specimen's top end. Accordingly, the 6-DOF control system is capable of applying bidirectional lateral drifts at the top of a beam-column specimen coupled with compressive axial load. Additionally, the 6-DOF control system can simulate almost any type of boundary conditions at the column top end.

The testing program involved ten 4-meter (L=13 feet) long wide-flange beam-column specimens that utilized W610 (W24) cross-sections. The testing matrix is summarized in Table 1 including the measured yield stress (F_y) and ultimate stress (F_u) of the corresponding steel material (A992 Gr-50 as per [8]). The W610 (W24) cross-sections are commonly found in steel special moment frames (SMFs) [9, 10]. The nominal geometric properties as well as the expected axial strength (P_y) and plastic flexural strength (M_p) of the cross-sections are summarized in Table 2. At 20% P_y, both cross-sections are considered to be seismically compact as per ANSI/AISC 341-10 [1]. From Table 2, both cross-sections have similar flange slenderness ratios ($b_f/2t_f$=5.9) but different web slenderness ratios (h/t_w). This was done intentionally in order to assess the effect of web slenderness ratio on the cyclic behavior of beam-columns. Past analytical studies [4, 11] indicated that this ratio is more critical than the local flange slenderness ratio. Furthermore, the two cross-sections have two different global slenderness ratios, L_b/r_y (i.e., L_b is the laterally unsupported length; r_y is the weak-axis radius-of-gyration of the column cross-

section). This allows us to assess the adequacy of the current L_b/r_y limit of ~60 in the current Canadian seismic provisions [2].

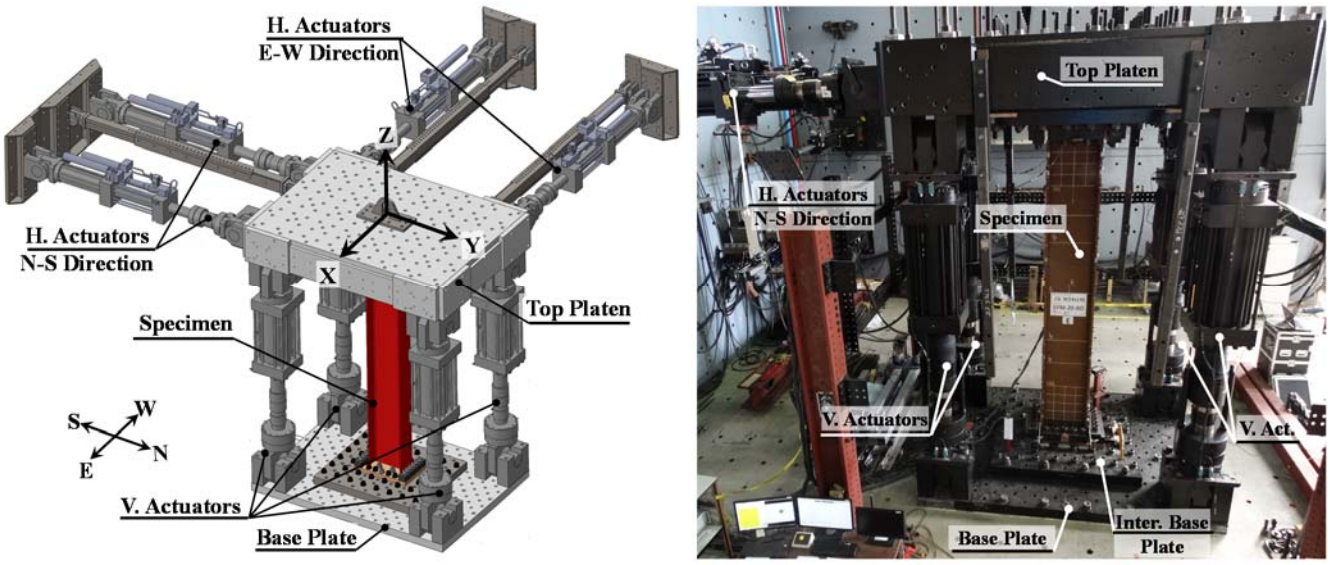

Fig. 1 – Overview of the 6-DOF test setup at EPM

Table 1 – Test matrix summary

Specimen ID	Section Size	Measured material properties		Lateral Protocol	P/P_y	BCs in the Strong-axis
		F_y [MPa]	F_u [MPa]			
C1	W610x217 (W24x146)	415	505	AISC-Symmetric (Unidirectional)	-0.2	Fixed-Fixed
C2				AISC-Symmetric (Unidirectional)	-0.5	
C3				AISC-Symmetric (Unidirectional)	-0.2	Fixed-Flexible
C4				Collapse-Consistent (Unidirectional)	-0.2	
C5		373	481	Collapse-Consistent (Unidirectional)	-0.2	
C6				AISC-Symmetric (Bidirectional)	-0.2	
C7	W610x125 (W24x84)	338	507	AISC-Symmetric (Unidirectional)	-0.2	
C8				Collapse-Consistent (Unidirectional)	-0.2	
C9				AISC-Symmetric (Bidirectional)	-0.2	
C10				Collapse-Consistent (Bidirectional)	-0.2	

From Table 1, the ten beam-column specimens were subjected to cyclic lateral drifts at their top end combined with a constant compressive axial load. Seven specimens were subjected to unidirectional lateral loading while three specimens were subjected to bidirectional loading. Two types of loading protocols were utilized: (a) a symmetric protocol (noted here as "SYM") and (b) a collapse-consistent protocol (noted here as "CPS"). The CPS protocol is representative of the ratcheting behavior of a frame building prior to collapse [12, 13]. The utilized unidirectional SYM loading protocol is similar to the one specified in ANSI/AISC 341-10 [1] for the pre-qualification of fully-restrained beam-to-column moment connections. The unidirectional CPS protocol developed by Suzuki and Lignos [14] is utilized here. The bidirectional SYM and CPS lateral loading protocols were developed using 3-dimensional nonlinear response-history analysis of a 4-story archetype steel frame building with perimeter SMFs [15]. From Table 1, except for one Specimen C2, a constant compressive axial load of 20% P_y was applied.

Table 2 – Nominal geometric properties and expected axial and flexural strength of the selected cross-sections

Column size	h/t_w	$b_f/2t_f$	r_y [mm]	L_b/r_y	P_y [kN]	M_p [kN.m]
W24x146	33.2	5.9	76.2	51	10520	2598
W24x84	45.9	5.9	18.3	79	6045	1392

Specimens C1 and C2 had fixed boundary conditions at both ends as summarized in Table 1. Specimen C3 to C10 had flexible boundary conditions at their top end (noted as fixed-flexible). The flexible boundary conditions were simulated about the specimen's strong-axis by applying a pre-defined rotation (θ_x) at the column top. During the elastic cycles of the applied lateral loading protocol, the inflection point is located at 0.75 L measured from the beam-column base. Fixed boundary conditions were applied at both ends of the columns with respect to their weak-axis. This assumption should be re-examined in future experimental studies because it affects the warping and torsional restraints of the column.

3. Steel Column Damage Progression

This section discusses the typical damage progression observed in one of the tested beam-column specimens. In particular, Specimen C10 is selected. This specimen utilized a W610x125 cross-section and was subjected to a bidirectional CPS lateral loading protocol combined with 20% P_y in compressive axial load.

Figure 2a shows the history of the lateral displacement applied at the column top (δ_y). Key damage states are indicated in the same figure such as: (a) the onset of local buckling (LB), (b) the flexural strength of the beam-column when reaching 80% of its maximum flexural capacity, (c) axial shortening (δ_z) reaching 1% L, (d) out-of-plane lateral deformations (δ_x) reaching 1% L, (e) onset of cross-section twisting; 1 degree beam-column cross-section rotation about the Z-axis (θ_z). Figure 2b shows the inflection point location (L_i) in the strong-axis loading direction, normalized by the column length L, versus the chord-rotation θ_{YZ}. The inflection point location, was monitored using the measurements of 54 uniaxial strain gauges installed along the height of the specimen. Fig.2c and Fig.2d show the moment-chord rotation relation at the beam-column base and top, respectively. Fig.2e shows the history of the axial displacement at the beam-column top, normalized by the beam-column length, versus the chord-rotation θ_{YZ}. Finally, Fig.2f and Fig.2g show the local and global deformation profiles, respectively, at the end of the test (chord-rotation of 9.2% rads).

The flanges of Specimen C10 yielded at 0.8% rads followed by the web at 1% rads during the first two cycles at 1.5% rads. During these cycles, the inflection point was located at 0.74 L as targeted (see Fig.2b). From Fig.2a, local buckling initiated in the flanges at the beam-column base at 1.5% rads. This can also be observed from the moment-rotation relations shown in Fig.2c. After the onset of local buckling at the column base (i.e., during the first excursion of 5% rads), the inflection point moved downwards L_i=0.3L (see Fig.2b). This resulted to an increase of the flexural demands at the beam-column top. Local buckling occurred at the beam-column top at the peak of the 5% drift excursion. At this point the inflection point started moving upward again. By the end of the test, after the plastification of both beam-column ends, the inflection point was located about the mid-height of the beam-column (L_i=0.5L). Overall, Specimen C10 was able to develop its plastic flexural capacity (i.e., M_{max}=1.05M_p). Specimen C10 was subjected to a maximum lateral chord-rotation of 9.2% and 3% rads in the strong- and weak-axis directions, respectively. By the end of the test, the beam-column base flexural strength reached zero while that of the top was half of its maximum flexural capacity (see Figs.2c and 2d).

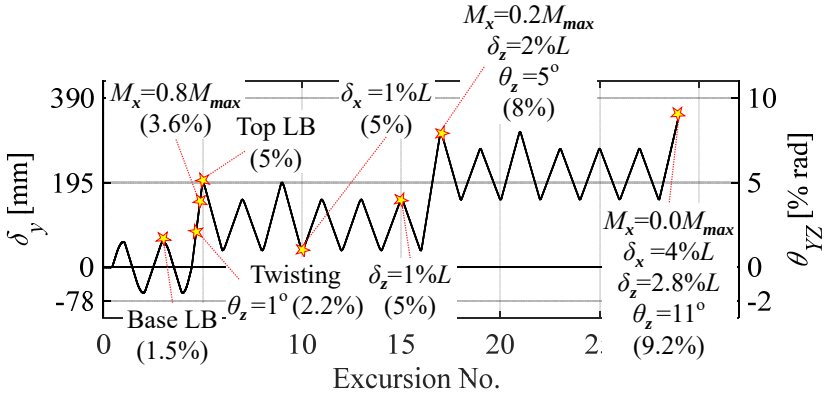

(a) displacement and chord-rotation history in the strong-axis

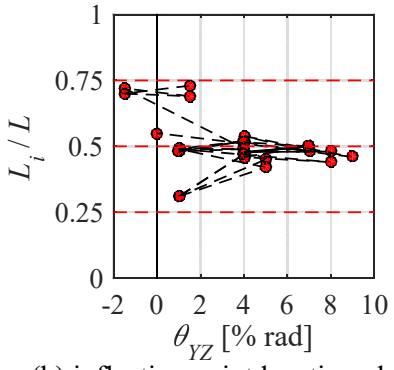

(b) inflection point location-chord rotation

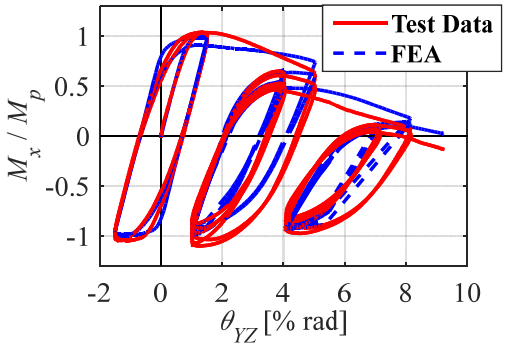

(c) moment versus chord at column base

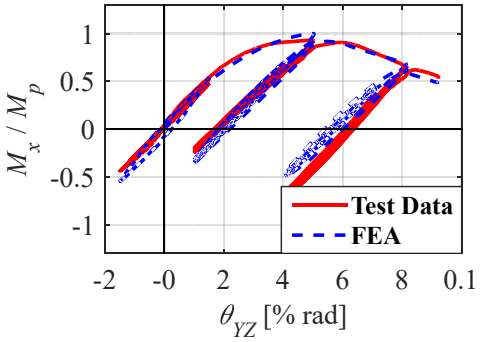

(d) moment versus rotation at column top

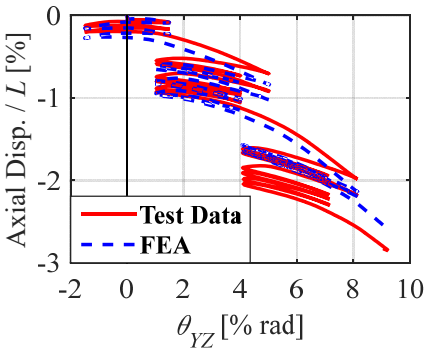

(e) normalized axial displacement versus chord rotation

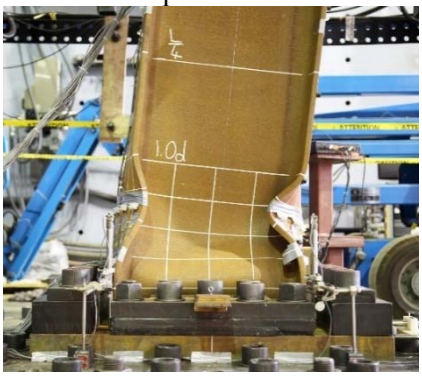

(f) local deformation profile at 9.2% rads (East view)

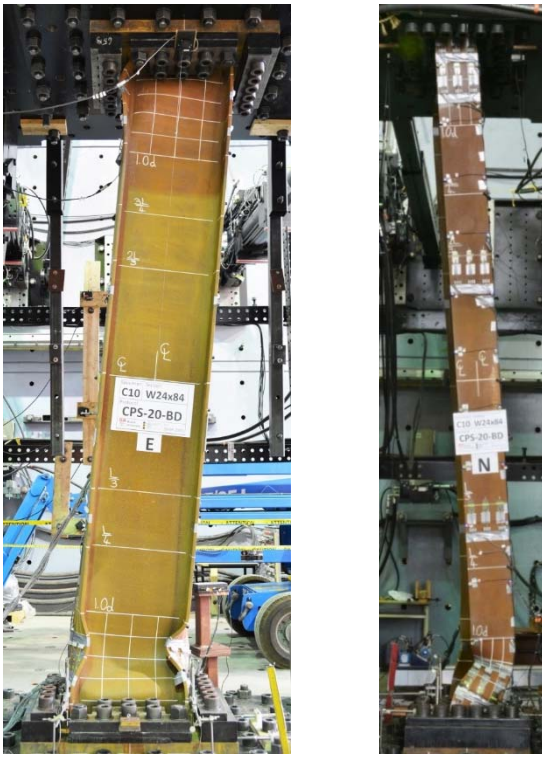

(g) global deformation profile at 9.2% rads

Fig. 2 – Damage progression in Specimen C10: W610x125 beam-column subjected to bidirectional collapse-consistent lateral loading protocol coupled with axial load of 20% P_y

Beam-column twisting was observed (θ_z=1°) during the first 5% drift excursion. Note that Specimen C10 experienced a peak drift ratio equal to 3% radians in its weak-axis orientation (i.e., the XZ plane) synchronized with the 5% drift amplitude in the strong-axis orientation. Following the second 5% drift excursion in the strong-axis direction, local buckling became more severe and beam-column axial shortening reached 1% L. At this point, out-of-plane lateral deformations (δ_x=1% L) were observed near the plastic hinge region at the beam-column base. At the end of the test, Specimen C10 shortened by 2.8% L due to severe web local buckling as shown in Fig.2e. Based on the white grid shown in Fig.2f, the peak of the local buckling cycle was at 0.7 d measured from the beam-column base, where d is the beam-column depth. The plastic hinge length at the beam-column base extended up to 1.6d. Specimen C10 also experienced a large twisting angle equal to 11° at the end of the test (see Fig.2g). Consequently, the initial elastic flexural stiffness of the specimen deteriorated by more than 60% (see Fig.2c). More details can be found about the behavior of the rest of the specimens can be found in [15].

4. Finite Element Modeling

An extensive finite element (FE) parametric study was conducted to investigate several aspects related to the hysteretic behavior of steel wide-flange beam-columns. To this end, a detailed finite element modeling approach was utilized. The modeling approach considers material nonlinearity and residual stresses commonly found in hot-rolled sections. The FE modeling approach was validated with the experimental data from the full-scale testing program discussed in Section 3. Sample comparisons of the deduced moment-rotation relations and the ones predicted by FEA are shown in the Figs. 2(c) and 2(e). Sample comparisons of the local and global deformation profiles between tests and FE models are shown in Fig.3. More details can be found in [15]. The FE modeling approach was also validated with past experimental studies on wide-flange beam-columns [4]. Overall, the FE modeling approach is able to capture with reasonable accuracy the nonlinear behavior as well as local and global instabilities of steel beam-columns regardless of the employed cross-section, geometry, boundary conditions and the applied loading protocol.

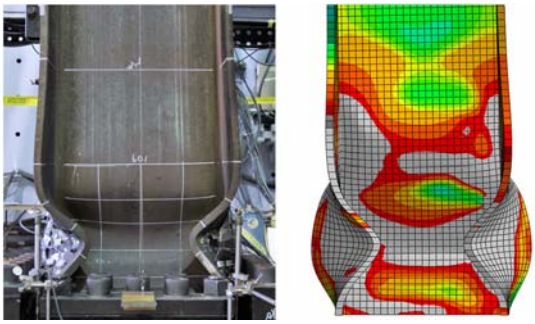

(a) Specimen C2

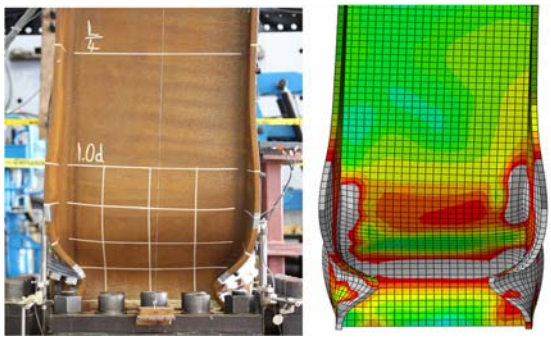

(b) Specimen C9

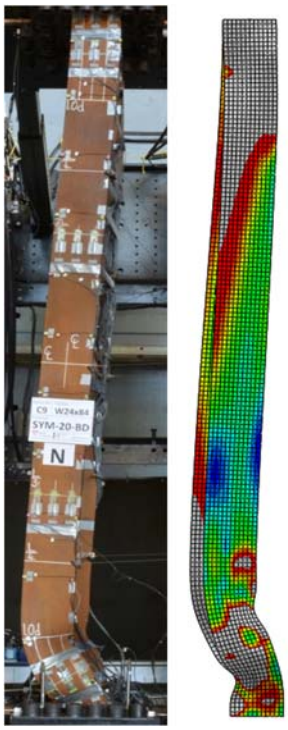

(c) Specimen C9

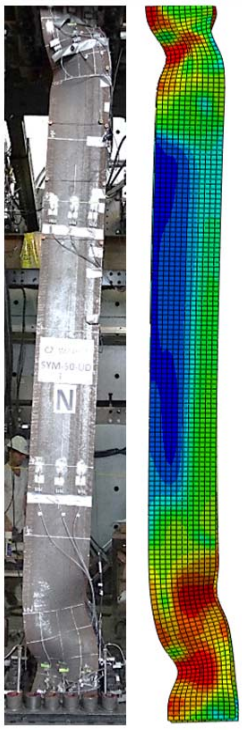

(d) Specimen C2

Fig. 3 – Comparison of simulated and observed deformation profiles

Using the FE modeling approach, the nonlinear behavior of 40 deep steel wide-flange cross-sections was investigated. A 4.6m (15 ft) long beam-column with fixed-flexible boundary conditions was considered for this purpose. The 40 cross-section sizes range from W410 (W16) to W920 (W36). To facilitate the interpretation of the FE results in the following sections, the 40 selected cross-sections were divided into four sets based on their corresponding web slenderness ratios. In brief, set W1 represents cross-sections with the lowest web slenderness ratios (i.e., $12.1 \leq h/t_w \leq 22$). Set W2 represents cross-sections with moderate web slenderness ratios ($22 \leq h/t_w \leq 32.5$). Set W3 represents cross-sections with web slenderness ratios close to the compactness limits for highly ductile steel members (λ_{hd}) (i.e., $32.5 \leq h/t_w \leq 43$) according to [1]. Set W4 represents five compact (λ_{md}) cross-sections according to ANSI/AISC 3641-10 [1] compactness requirements for moderately ductile members (i.e., $43 \leq h/t_w \leq 57.5$). Note that the two cross-sections utilized in the experimental program (i.e., W610x217 and W610x125) belong to set W3.

5. Discussion

This section summarizes the main findings related to the hysteretic behavior of wide-flange beam-columns based on a synthesis of the experimental results as well as the FE parametric study.

5.1 Effects of bidirectional/unidirectional loading

Specimens C8 and C10 utilized the same cross-sections, boundary conditions, and applied axial compressive load (see Table 1). The hysteretic behavior of the two specimens is compared in terms of their deduced moment-rotation relation and the corresponding first-cycle envelope curve as shown in Figs.4a and 4b, respectively. Fig.4 shows that the plastic deformation capacity of a beam-column is practically not sensitive to the bidirectional lateral loading. This observation holds true for the range of sections that were tested regardless of the type of lateral loading (i.e., symmetric or collapse-consistent). Nonetheless, for story drift-ratios larger than 3% radians, the rate of cyclic deterioration in flexural strength of a beam-column is slightly larger under bidirectional lateral loading compared to that from unidirectional lateral loading. This is attributed to the additional flexural demands in the weak-axis direction of the beam-column cross section. This effect is practically negligible on the first-cycle envelope curves of the same specimens shown in Fig.4b. In that respect, if the objective is to construct a first-cycle envelope curve for beam-columns for the nonlinear evaluation of steel MRFs under seismic loading this can be done with experimental data based on unidirectional loading protocols.

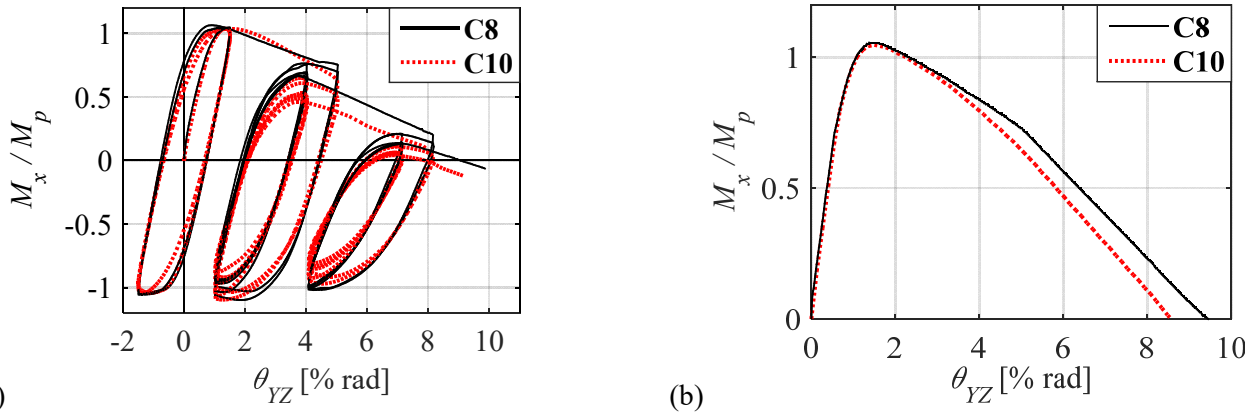

Fig. 4 – Comparison between Specimens C8 and C10: (a) normalized moment-rotation relation at beam-column base; (b) first-cycle envelope curve

From Fig.4a, for chord-rotations larger than 3% radians the unloading stiffness of a beam-column that is subjected to bidirectional symmetric lateral loading deteriorates more compared to that from unidirectional lateral loading. This is attributed to the magnitude of out-of-plane deformations of the steel

column under bidirectional lateral loading compared to those under unidirectional lateral loading. This was more evident for W610x125 beam-columns (i.e., L_b/r_y = 79) compared to the W610x217 beam-columns (i.e., L_b/r_y = 51). The aforementioned observations are sensitive to the number and amplitude of inelastic cycles that a beam-column experiences as discussed in the next section.

5.2 Effects of loading protocol

Figures 5a and 5b show comparisons between Specimen C3 and C5 in terms on moment-rotation and axial displacement-rotation relations, respectively. Specimen C3 and C5 were nominally identical but were subjected to a different type of lateral loading protocol (see Table 1). Fig. 5a shows that, regardless of the loading protocol, both specimens developed almost the same amount of cyclic hardening (i.e., M_{max}/M_p=1.0). However, the hysteretic behavior between the two specimens differed substantially. From Fig. 5a, Specimen C5 had nearly double plastic rotation capacity compared to that of Specimen C3. This is attributed to the number of inelastic cycles of a symmetric lateral loading protocol compared to those of a collapse-consistent loading protocol. For the same reason, the amount of axial shortening that Specimen C5 experienced was about three times less than that from Specimen C3 (see Fig.5b). For instance, at 5% radians, Specimen C5 shortened by 0.6% L while Specimen C3 shortened by 4% L (see Fig.5b).

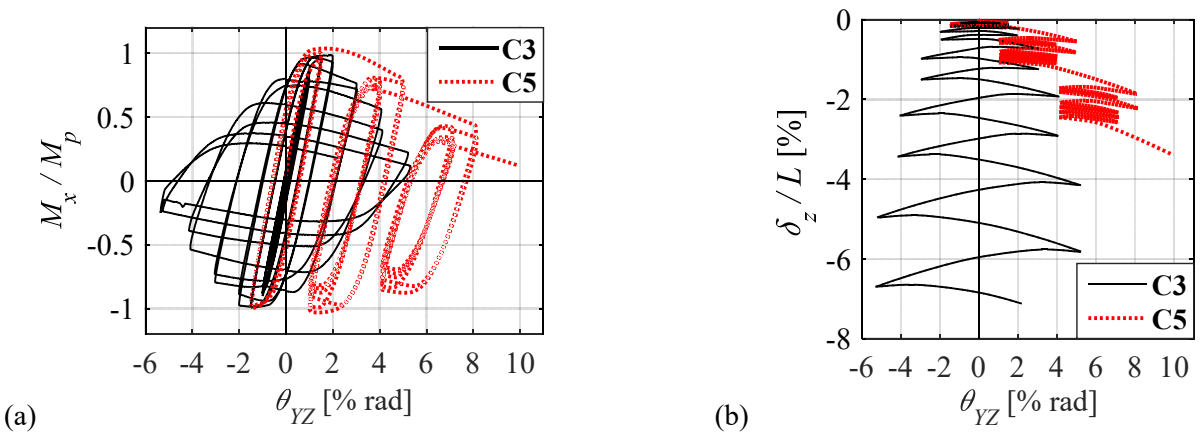

Fig. 5 – Comparison between Specimens C3 and C5: (a) normalized moment versus chord-rotation at beam-column base; (b) normalized axial displacement versus chord-rotation

The observations discussed above were generalized based on the FE parametric study that was conducted. In particular, Fig. 6a shows the ratio of cyclic hardening (i.e., M_{max}/M_p) developed by the 40 beam-column cross-sections versus the web slenderness ratio when subjected to the SYM and CPS lateral loading protocols. From this figure, the observed cyclic hardening of beam-columns is not sensitive to the employed lateral loading protocol regardless of the cross-section web slenderness ratio.

The cyclic deterioration in flexural strength of a steel column is further quantified based on the chord-rotation at which 20% M_{max} is reached (i.e., $\theta_{20\%Mmax}$). Fig. 5b shows the ratio of $\theta_{20\%Mmax}$ from columns subjected to the SYM protocol to that measured from the CPS protocol versus the column web slenderness ratio. From this figure, $\theta_{20\%Mmax}$ based on the SYM protocol is on average 50% lower than that of the CPS protocol regardless of the web local slenderness of the steel column cross-section.

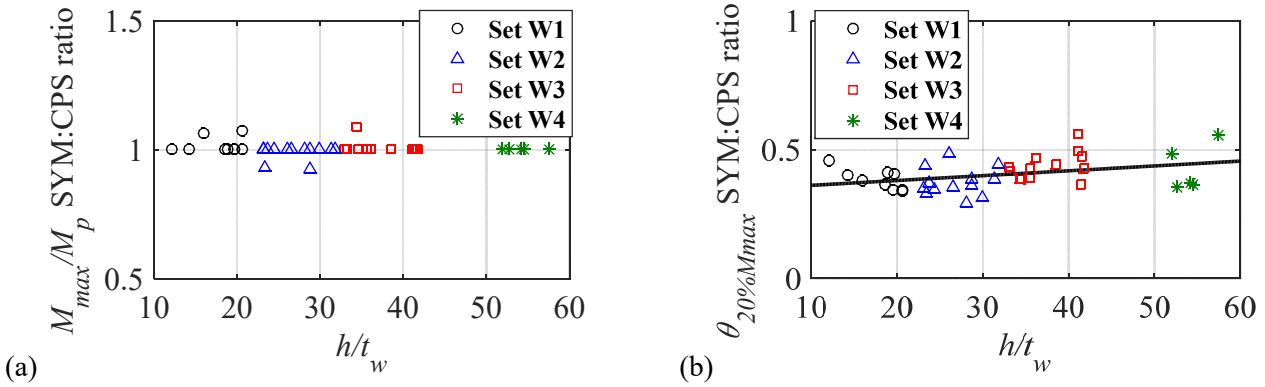

Fig. 6 – (a) ratio of cyclic hardening measured from SYM protocol to that of the CPS protocol versus web slenderness ratio (b) ratio of chord-rotation at 20% M_{max} of the SYM protocol to that of the CPS protocol versus web slenderness ratio

5.3 Lateral bracing force

The steel specifications in North America [2, 7] provide empirical equations to calculate the axial design force for bracing members. In particular, for steel MRF columns, Clause 9.2.5 of CAN/CSA S16-09 [2] specifies a lateral brace axial strength (P_b) equal to at least 2% of the factored compressive force C_f as given by Eq. (1), in which R_y is a factor applied to estimate the probable yield stress (taken as 1.1), f_{yn} is the nominal yield stress of the steel material, and A_{comp} is the cross-sectional area in compression. Similarly, Section 6.4 of ANSI/AISC360-10 [7] specifies that the axial strength of a nodal brace (P_{rb}) be calculated as given by Eq. (2), in which P_r and M_r are the required axial and flexural strength of the beam-column, respectively, h_o is the distance between flange centroids, and C_d =2.0 for braces closest to the beam-column inflection point. Note that the "nodal brace" design force is more conservative compared to the lower "relative brace" design force also specified by [7].

$$P_b = 0.02\ C_f = 0.02 * R_y f_{yn} A_{comp} \quad (1)$$

$$P_{rb} = 0.01\ \mathrm{P_r} + 0.02\ M_r\ C_d / h_o \quad (2)$$

In this section, the adequacy of Equations 1 and 2 is assessed. To this end, the reaction force (noted as P_{brace}) at the beam-column specimens top end was monitored. Fig. 7a shows the history of the lateral force in the X-axis direction (P_{brace}), normalized by the measured axial yield strength P_y, for Specimen C1 (see Sections 2 and 3). In the same figure, the brace design axial force as calculated per [2] and [7] is superimposed. From this figure, Specimen C1 developed a maximum P_{brace} force equal to 1.75% P_y. At chord-rotations larger than 2% rads the brace design force as per [2] and [7] is exceeded. This observation holds true for all specimens utilizing a W610x217 cross-section (L_b/r_y=51). In average, the same specimens developed a maximum force of 1.7% P_y. On the other hand, beam-column specimens that utilized a W610x125 cross-section (L_b/r_y=79) developed, on average, a lower maximum force equal to 0.9% P_y. This level of force did not exceed the design forces as per [2] and [7]. This is attributed to the small torsional resistance of the same specimens.

The correlation between local and global slenderness ratios and the lateral brace force is further investigated based on the FE parametric study. Figure 7b shows the normalized P_{brace} as predicted by the FEA versus the global slenderness ratio L_b/r_y for the 40 members that were analyzed as part of the FE parametric study. The unbraced length, L_b, is the same for all 40 beam-columns (i.e., L_b=4600mm) because lateral bracing is only provided at the floor level. The L_b/r_y limit (i.e., L_b/r_y~60) specified in [2] is superimposed in the same figure. Note that the data plotted in Fig.7b are based on a symmetric lateral loading combined with an axial load of 20% P_y. Also note that the P_{brace} values are the maximum forces measured up to a reference chord-rotation of 4% radians. From Fig.7b, there is a strong correlation between the lateral brace force demand and the L_b/r_y ratio. The larger the L_b/r_y, the smaller the out-of-plane lateral force demands. At 20% P_y, stocky beam-columns ($12.1 \leq h/t_w \leq 22$) that typically have $L_b/r_y < 60$ seem to reach out-of-plane force demands up to 6% P_y on the lateral bracing. From the same figure,

beam-columns with $32.5 \leq h/t_w \leq 43$ that have a $L_b/r_y < 60$ reach out-of-plane force demands up to 2% P_y. This agrees with the experimental findings that were briefly discussed in Section 3. Although not shown here due to brevity, a correlation between the out-of-plane force demands and the applied axial load level is also observed. In particular, the higher the applied compressive axial load the lower the P_{brace} force. This is attributed to the fact that local buckling becomes the controlling failure mode at higher axial loads over geometric instabilities associated with global and lateral torsional buckling. Additionally, at higher axial loads, most of the beam-column lost their flexural strength at lower chord-rotations before significant out-of-plane forces develop.

Figures 8a and 8b show the ratio of the predicted brace force (P_{brace}) normalized with respect to P_b as per [2] and P_{rb} as per [7], respectively, versus L_b/r_y. From Fig.8, highly compact beam-columns (i.e., sets W1 and W2) subjected to axial loads of 20% P_y experience lateral brace force demands that exceed the lateral brace design forces as per [2] and [7]. In particular, P_{brace} may reach more than 4 times P_b and more than 2 times P_{rb}. For high axial load ratios (i.e., P/P_y =0.5), the lateral bracing force demand is always less than 2% P_y. However, this level of axial load is not of interest for new steel frame buildings. The reason is that in Type D steel MRFs, the applied axial load ratio on steel columns is limited to 0.30 (see Clause 27.2.3.1, [2]). In summary, the design force as per [2] and [7] for lateral bracing of beam-columns should be re-assessed.

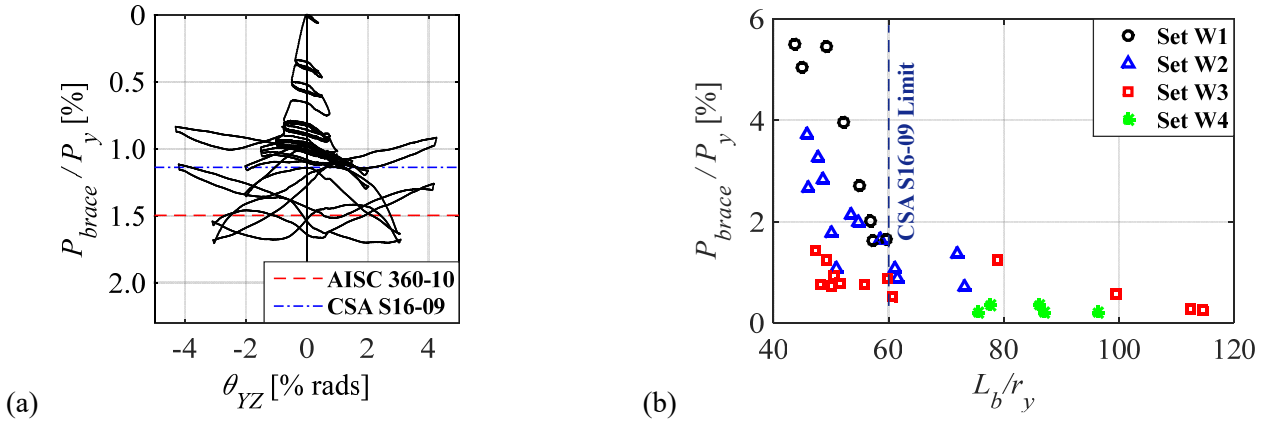

Fig. 7 – (a) Specimen C1: normalized out-of-plane force versus true chord-rotation; (b) FE predicted brace force, normalized by P_y, versus global slenderness ratio

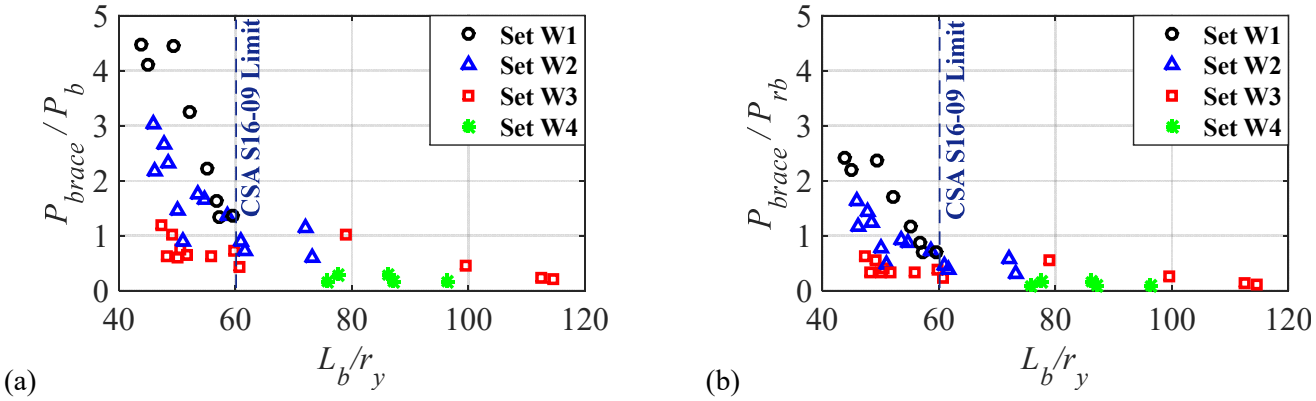

Fig. 8 – Ratio of predicted brace force to brace design force versus global slenderness ratio (left CSA S16-09 [2], right ANSI/AISC 360-10 [7])

6. Conclusions

This paper discusses the findings from a full-scale testing program and a corroborating FE parametric study on deep steel wide-flange beam-columns. The testing program involved ten W610 specimens that were tested under bidirectional and unidirectional lateral loading protocols representative of design-basis and collapse consistent

seismic events. The beam-column specimens had a fixed base and flexible top end in order to better represent the boundary conditions of interior first-story columns in steel MRFs. The FE modeling approach was validated with the experimental data. The nonlinear cyclic behavior of 40 wide-flange cross-sections was investigated as part of a typical interior first-story steel MRF column. The main observations from the experimental program and the FE parametric study are summarized as follows:

- At story drift ratios less than 3%, the effect of bidirectional loading on the cyclic behavior of steel beam-columns is negligible. At larger story drift ratios, beam-columns subjected to bidirectional loading develop a plastic rotational capacity that is 10% less compared to nominally identical columns subjected to unidirectional lateral loading.
- Out-of-plane global instabilities are triggered earlier when a beam-column is subjected to bidirectional lateral loading compared to unidirectional lateral loading. This is more evident in beam-columns with large global slenderness ratios (L_b/r_y~79).
- Beam-columns subjected to a collapse-consistent lateral loading protocol achieve almost double plastic deformation capacity compared to nominally identical columns subjected to a symmetric lateral loading protocol. This is attributed to the large number of inelastic cycles included in the latter.
- At a reference story drift ratio of 4% rads, beam-columns subjected to a collapse-consistent protocol shortened on average by 1% L, which was about 5 times less than that measured in nominally identical columns subjected to a symmetric lateral loading protocol.
- Beam-columns with local slenderness ratios close to the compactness limits for highly ductile members as per [1] (i.e., $32.5 \leq h/t_w \leq 43$) and global slenderness ratio, L_b/r_y, less than 60 develop out-of-plane force demands up to 2% P_y on the lateral bracing. The out-of-plane force demands can reach up to 6% P_y for stocky cross-sections ($12.1 \leq h/t_w \leq 22$).
- At story drift ratios less than 2% rads, the lateral bracing design axial force per [2] and [7] is adequate for beam-columns that utilize a W24x146 cross-section ($h/t_w < 33$ and $L_b/r_y < 52$). For story drift ratios larger than 4% radians, the lateral bracing design axial forces as per [2] and [7] are exceeded. Accordingly, the lateral bracing design axial force per [2] and [7] should be re-assessed.

7. Acknowledgements

This study is based on work supported by the National Science and Engineering Research Council of Canada (NSERC) under the Discovery Grant Program. The Steel Structures Education Foundation (SSEF) also provided funding for the testing program. The financial support is gratefully acknowledged. The ADF Corporation Inc. donated the material and fabrication for four of the specimens. The authors would like to sincerely thank Prof. Robert Tremblay, École Polytechnique de Montréal (EPM), for providing the opportunity to use the 6-DOF test setup and resources at EPM. The authors sincerely thank the technical staff at the EPM structures laboratory: Martin Leclerc, Romain Siguier, Xavier Willem, Patrice Bélanger, and David Ek, as well as the graduate and undergraduate students: Julien Cravero, Paul Bessieres, and Ahmed Khanafer for their invaluable assistance during the testing program. Any opinions, findings, and conclusions or recommendations expressed in this paper are those of the authors and do not necessarily reflect the views of sponsors.

8. References

[1] AISC. *Seismic provisions for structural steel buildings*, *ANSI/AISC 341-10*. American Institute for Steel Construction: Chicago, IL, 2010.

[2] CSA. *Design of steel structures*, *CAN/CSA S16-09*. Canadian Standards Association: Mississauga, Canada, 2009.

[3] Uang, C.-M., Ozkula, G., and Harris, J. (2015): Observations from cyclic tests on deep, slender wide-flange structural steel beam-column members. *The Annual Stability Conference, Structural Stability Research Council (SSRC)*. Nashville, Tennessee, USA.

[4] Elkady, A. and Lignos, D.G. (2015): Analytical investigation of the cyclic behavior and plastic hinge formation in deep wide-flange steel beam-columns. *Bulletin of Earthquake Engineering*; **13**(4), 1097-1118. DOI: 10.1007/s10518-014-9640-y.

[5] Fogarty, J. and El-Tawil, S. (2015): Collapse resistance of steel columns under combined axial and lateral loading. *Journal of Structural Engineering*. DOI:10.1061/(ASCE)ST.1943-541X.0001350.

[6] Newell, J.D. and Uang, C.-M. Cyclic behavior of steel columns with combined high axial load and drift demand. *Report No. SSRP-06/22*, Department of Structural Engineering, University of California, San Diego, 2006.

[7] AISC. *Specification for structural steel buildings*, *ANSI/AISC 360-10*. American Institute for Steel Construction: Chicago, IL, 2010.

[8] ASTM. *Standard specification for structural steel shapes*, *ASTM A992 / A992M-11*. ASTM International: West Conshohocken, PA, USA, 2015.

[9] Elkady, A. and Lignos, D.G. (2014): Modeling of the composite action in fully restrained beam-to-column connections: implications in the seismic design and collapse capacity of steel special moment frames. *Earthquake Engineering & Structural Dynamics*; **43**(13), 1935-1954. DOI: 10.1002/eqe.2430.

[10] NIST. Evaluation of the fema p695 methadology for quantification of building seismic performance factors. *NIST GCR 10-917-8*, NEHRP consultants Joint Venture, 2010.

[11] MacRae, G.A., Carr, A.J., and Walpole, W.R. The seismic response of steel frames. *Report No. 90-6*, Department of Civil Engineering, University of Canterbury, New Zealand, 1990.

[12] Ibarra, L.F. and Krawinkler, H. Global collapse of frame structures under seismic excitations. *Report No. 152*, The John A. Blume Earthquake Engineering Center, Stanford University, Stanford, CA, 2005.

[13] Lignos, D.G., Krawinkler, H., and Whittaker, A.S. (2011): Prediction and validation of sidesway collapse of two scale models of a 4-story steel moment frame. *Earthquake Engineering & Structural Dynamics*; **40**(7), 807-825. DOI: 10.1002/eqe.1061.

[14] Suzuki, Y. and Lignos, D.G. (2014): Development of loading protocols for experimental testing of steel columns subjected to combined high axial load and lateral drift demands near collapse. *10th National Conference on Earthquake Engineering (10th NCEE)*. Anchorage, Alaska, USA. DOI:10.4231/D3M32N99R

[15] Elkady, A. and Lignos, D.G. (2016): Dynamic stability of deep and slender wide-flange steel columns – full scale experiments. *The Annual Stability Conference (NASCC)*. Orlando, Florida, USA.